remote sensing

MDPI

Article

Significant Inverse Influence of Tropical Indian Ocean SST on SIF of Indian Vegetation during the Summer Monsoon Onset Phase

Roma Varghese [1], Swadhin K. Behera [2] and Mukunda Dev Behera [1,*]

[1] Centre for Ocean, River, Atmosphere and Land Sciences, Indian Institute of Technology Kharagpur, Kharagpur 721302, India
[2] Applications Laboratory, Japan Agency for Marine-Earth Science and Technology, Yokohama 236-0001, Japan
* Correspondence: mdbehera@coral.iitkgp.ac.in

Abstract: Sea surface temperature (SST) substantially influences the land climate conditions through the co-variability of multiple climate variables, which in turn affect the structural and functional characteristics of terrestrial vegetation. Our study explored the varying responses of vegetation photosynthesis in India to the SST variations in the tropical Indian Ocean during the summer monsoon. To characterise the terrestrial photosynthetic activity, we used solar-induced chlorophyll fluorescence (SIF). Our results demonstrated a significant negative SST-SIF relationship during the onset phase of the summer monsoon: the SIF anomalies in the northern and central Indian regions decrease when strong warm SST anomalies persist in the tropical Indian Ocean. Further, SIF anomalies increase with cold anomalies of SST. However, the negative SST anomalies in the tropical Indian Ocean are less impactful on SIF anomalies relative to the positive SST anomalies. The observed statistically significant SST–SIF link is feasible through atmospheric teleconnections. During monsoon onset, positive SST anomalies in the tropical Indian Ocean favour weakened monsoon flow, decreasing moisture transport from the ocean to the Indian mainland. The resultant water deficiency, along with the high air temperature, created a stress condition and reduced the photosynthetic rate, thus demonstrating negative SIF anomalies across India. Conversely, negative SST anomalies strengthened monsoon winds in the onset period and increased moisture availability across India. Negative air temperature anomalies also dampen water stress conditions and increased photosynthetic activity, resulting in positive SIF anomalies. The identified SST-SIF relationship would be beneficial to generate a simple framework that aids in the detection of the probable impact on vegetation growth across India associated with the rapidly varying climate conditions in the Indian Ocean.

Keywords: sea surface temperature; solar-induced chlorophyll fluorescence; Indian vegetation; plant photosynthesis; ocean-vegetation interactions

Citation: Varghese, R.; Behera, S.K.; Behera, M.D. Significant Inverse Influence of Tropical Indian Ocean SST on SIF of Indian Vegetation during the Summer Monsoon Onset Phase. *Remote Sens.* **2023**, *15*, 1756. https://doi.org/10.3390/rs15071756

Academic Editor: Andrew Clive Banks

Received: 2 February 2023
Revised: 4 March 2023
Accepted: 21 March 2023
Published: 24 March 2023

1. Introduction

Sea surface temperature (SST), the essential geophysical variable that provides information about the ocean surface heat, is a key element in determining the earth's climate [1]. This fundamental oceanic variable substantially influences our planet's weather and climate patterns by regulating dynamic and biogeochemical processes linking the ocean with the atmosphere [2]. SST is used as a simple and sensible indicator to understand complex air-sea interactions and their implications on the earth's surface [3]. In conjunction with surface air temperatures, SST variations can create intensified extreme climate phenomena that trigger severe economic and agricultural losses [4]. Some regional SST anomalies control the photosynthetic assimilation of carbon in terrestrial ecosystems by altering heat and moisture fluxes through the atmospheric bridge [5,6]. Climatic oscillations such as the El Niño Southern Oscillation (ENSO), Indian Ocean Dipole (IOD), Pacific Decadal

Oscillation (PDO) and Atlantic Multidecadal Oscillation (AMO) affect global vegetation through teleconnections, establishing the relevance of oceanic contribution to the terrestrial ecosystem functioning [7–9]. Hence, a detailed study of the relationship between SST and terrestrial photosynthesis should be conducted to understand the vegetation response to ocean variability [10].

Solar-induced chlorophyll fluorescence (SIF) is an innovative measure of photosynthetic activity that offers a physiological proxy of vegetation gross primary productivity (GPP) [11,12]. SIF serves as a better indicator of actual plant photosynthesis because of its direct mechanistic connection to the internal photosynthetic systems rather than an indicator of vegetation greenness as in traditionally used vegetation indices (VIs) [13–15]. SIF captures variations in vegetation's photosynthetic activity and thus reflects the plant's physiological state in real-time rather than waiting for its visible changes to come [16]. SIF retrievals trace the response of vegetation functioning to dynamic environments and help to understand, quantify and predict the corresponding anomalies in vegetation [17]. This radiation flux re-emitted by plants from chlorophyll molecules excited during photosynthesis in the red and far-red bands of the electromagnetic spectrum (650–850 nm) with peaks at 685 nm and 740 nm is a small portion of absorbed photosynthetically active radiation, which requires sensitive instruments of sub-nanometer spectral resolution and high signal-to-noise ratio to capture [18]. SIF goes one step ahead of the reflectance-based VIs as a surrogate measure of GPP [19] as it responds rapidly to changes in environmental factors, especially to stress [20]. Remote sensing of SIF from space using atmospheric spectrometers greatly improved tracking vegetation photosynthesis at various spatial and temporal scales [21]. It thus became widely useful in agricultural and forestry fields, such as drought/stress detection, phenology monitoring and crop yield/productivity estimations [22–24].

SSTs act as a significant external control of land climate [25], consequently regulating the spatio-temporal distribution of climate variables that directly affect the vegetation's photosynthetic activity through physiological processes [26]. The West Pacific Warm Pool exerts a robust but variable influence on net ecosystem productivity in both the northern (positive correlation) and southern (negative correlation) hemispheres through modification of precipitation and land surface temperature [27]. Coupled CCM3-IBIS model demonstrated correlations of vegetation net primary productivity (NPP) across South America with SST of the surrounding oceans and simulated changes in the NPP under the IPCC A2 warming scenario for the first half of the 21st century [28]. The observational evidence based on satellite data and model simulations showed that SST variations mostly interact with photosynthesis through teleconnections and the associated co-variability patterns between multiple climate variables [29]. Therefore, SST indices have predictive skills on the variability of terrestrial photosynthesis due to the time lag between each link in this cause-effect chain, compared to the meteorological parameters (e.g., rainfall and air temperature) [30]. It is reported that using SSTs, vegetation greenness of the arid and semi-arid climatic zones across the tropical belt can be forecasted 3–6 months in advance [26]. The ocean-vegetation link demonstrates the possible impact of SST on the functional status of terrestrial ecosystems. Thus, the current study intends to investigate how the tropical Indian Ocean contributes to anomalies in vegetation photosynthesis over the Indian subcontinent using SIF and SST indices.

As an agrarian country with rich natural vegetation, India is surrounded by the Indian Ocean on three sides and experiences a monsoon climate [31–34]. It offers an ideal site to study the oceanic influence on vegetation anomalies. Since hydroclimatic fluctuations predominantly control plant growth and productivity [35,36], the majority of previous investigations focused on the effects of rainfall and temperature on various structural and functional characteristics of Indian vegetation [37–39]. Few studies used remote SST forcing to show the impact of ENSO on the inter-annual variability of vegetation productivity in India and attempted to illustrate the effect of climate variability on ecosystem services [40–42]. Asoka and Mishra (2015) showed the potential of predicting NDVI anomalies across India using soil moisture and the ENSO index [35]. Moreover, along with the

ENSO teleconnections, the variability of SST in the tropical Indian Ocean also contributes to the vegetation anomalies in India [9]. At the same time, there exists a paucity of active research on the role of SST variations in the tropical Indian Ocean in bringing changes in the functioning of the Indian terrestrial vegetation ecosystem. Besides, this study aims to evaluate the varying responses of vegetation photosynthetic activity in India to SST anomalies using SIF measurements based on advanced remote sensing techniques. The application of satellite-based SIF data products offers a unique opportunity to comprehend how exactly terrestrial vegetation photosynthesis is linked to Indian Ocean SSTs, which is not addressed in the previous studies. Indian Ocean SST variability also plays a critical role in the climate conditions over the Indian subcontinent, significantly influencing vegetation anomalies. Thus, our study provides a simple framework that can identify the anomalies in Indian vegetation photosynthetic activity that arise from the rapidly varying climate conditions in the Indian Ocean, and clearly, this is of huge agricultural and economic interest.

The present work focuses on the relationship between SST variations in the tropical Indian Ocean regions and SIF anomalies across the Indian mainland to understand the possible impacts of regional-scale SST anomalies on the photosynthetic activity of the nearby terrestrial ecosystem. The summer monsoon period (June–September) is critical to the vegetation over the Indian landmass as it plays a significant role in determining water availability [43]. Therefore, our analysis aims to explore the SST-SIF linkage exclusively for June, July, August and September. To account for the spatial variability of SST over the monsoon domain [44], the tropical Indian Ocean is divided into the Western Indian Ocean (WIO), Northern Indian Ocean (NIO) and Central Indian Ocean (CIO) following the spatial pattern of average seasonal SST during the summer monsoon (Figure 1). India experiences complex agro-climatic situations; hence, the country has been divided into different (homogeneous) agro-climatic zones (ACZs) based on physiography, soil, climate and vegetation by the Indian Planning commission [45]. India may be considered as having 14 mainland ACZs, such as the Western Himalayan Region (WHR), Trans Gangetic Plains (TGP), Upper Gangetic Plains (UGP), Middle Gangetic Plains (MGP), Lower Gangetic Plains (LGP), Eastern Himalayan Region (EHR), Western Dry Region (WDR), Central Plateau and Hills (CPH), Eastern Plateau and Hills (EPH), Gujarat Plain and Hills (GPH), Western Plateau and Hills (WPH), Southern Plateau and Hills (SPH), Western Coastal Plains and Ghats (WCPG) and Eastern Coastal Plains and Hills (ECPH) to eliminate the heterogeneity in terms of climate and vegetation types.

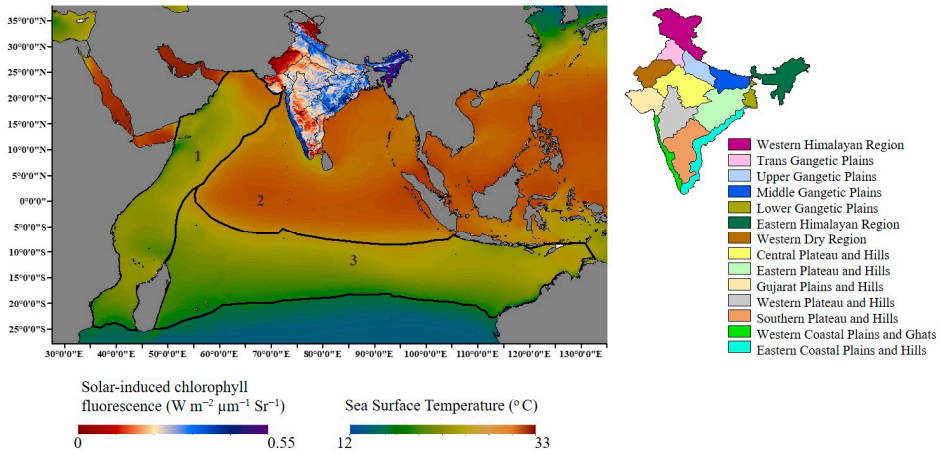

Figure 1. Shows the climatology of SIF (spatial resolution of 0.05 × 0.05-degree grid) across India and SST (spatial resolution of 0.25 × 0.25-degree grid) in the tropical Indian Ocean during the summer monsoon. Indian landmass is divided into 14 agro-climatic zones, and the tropical Indian Ocean is stratified into (1) Western, (2) Northern and (3) Central regions based on the SST pattern. (Software used: ArcMap version 10.3 (Esri Inc. (Redlands, CA, USA, 2014), https://desktop.arcgis.com/en/arcmap/ (accessed on 10 July 2021)).

2. Materials and Methods

2.1. Data

Gridded datasets of SIF, SST, specific humidity, air temperature, soil moisture, rainfall and wind components collected during 2001–2018 were used in the study (Table 1).

Table 1. Details of data used from 2001–2018 at monthly temporal resolution.

Data	Spatial Resolution (Deg)	Source
Solar-Induced chlorophyll Fluorescence	0.05 × 0.05	GOSIF V2
Sea Surface Temperature	0.25 × 0.25	NOAA OISST V2.1
Air Temperature at 2 m	0.5 × 0.625	MERRA-2 Model
Specific humidity at 850 hPa	0.5 × 0.625	MERRA-2 Model
Rainfall	0.25 × 0.25	IMD
Wind components at 850 hPa	0.25 × 0.25	ERA5
Soil Moisture	0.1 × 0.1	FLDAS Model
NINO3 SST and DMI	-	NOAA PSL GCOS

Global Orbiting Carbon Observatory SIF (GOSIF) version 2 data used in this study which was developed by integrating coarser Orbiting Carbon Observatory-2 (OCO-2) SIF retrievals at 757 nm, surface reflectance from the Moderate Resolution Imaging Spectroradiometer (MODIS) and reanalysis meteorological data from the Modern-Era Retrospective Analysis for Research and Applications (MERRA-2) using Cubist regression tree model, which is an extension of Quinlan's M5 model tree [46]. Approximately 2.6 million data points were used to train the model, which could encompass different climatic conditions and ecosystem types. This model predicted SIF fairly well across the globe (R^2 = 0.79, RMSE = 0.07 W m^{-2} μm^{-1} s^{-1}) with a continuous global coverage over 2000–2021, the longest length of SIF record available so far [47]. The predicted SIF has an improved spatial (0.05°) and temporal (8-day) resolution compared with other gridded SIF datasets (GOSAT and GOME-2) and a reasonable seasonal cycle which is similar to that of coarser-resolution OCO-2 SIF records [48]. GOSIF estimates are highly correlated with ground-based GPP from 91 eddy covariance flux sites (R^2 = 0.73, $p < 0.001$) across the globe [49]. Only a few studies explored the potential of SIF data to monitor the Indian terrestrial ecosystems [50], and it well-represented the vegetation anomalies across India during the monsoon period [51].

SST data were collected from the high-resolution product of the NOAA 0.25° daily Optimum Interpolation Sea Surface Temperature version 2 (OISST V2) [52]. OISST V2 is one of the most popular L4 datasets constructed by combining satellite and in-situ [53] on a regular global grid, with gaps filled in by the interpolation technique. The bias correction of satellite SSTs using in situ data is applied to compensate for any biases in the satellite data using the empirical orthogonal teleconnections method [54]. To represent the influence of ENSO, the NINO3 index was used in the study. NINO3 index is the SST anomalies averaged over 5°S–5°N & 150°W–90°W (Niño 3 region). This index was derived by calculating the monthly anomalies of Niño 3 region-averaged SST obtained from the global climate observing system of the Physical Sciences Laboratory (PSL) [55]. The intensity of IOD is measured by dipole mode index (DMI). Dipole mode index (DMI) is the SST anomaly (SSTA) difference between the tropical Western Indian Ocean (10°S–10°N & 50°E–70°E, IOD west) and the tropical South-eastern Indian Ocean (10°S–0°S & 90°E–110°E, IOD east) which is computed as DMI = $SSTA_{\text{IOD west}} - SSTA_{\text{IOD east}}$. The monthly DMI dataset was obtained from PSL [56].

Specific humidity and air temperature data (2 m) were obtained from the MERRA-2 model outputs [57]. The MERRA-2 data products have a horizontal resolution of 0.625° × 0.5° and can be retrieved from the Geovanni. Soil moisture data were obtained from the Famine Early Warning Systems Network (FEWS NET) land data assimilation system (FLDAS). FEWS NET offers soil moisture distribution products derived from the FLDAS Noah Land Surface Model L4 at 0.10° horizontal resolution on a monthly and

yearly basis [58]. We used high-resolution daily rainfall data from the India Meteorological Department (IMD) [59]. The recent IMD rainfall data is gridded at 0.25° spatial resolution, available for 120 years and arranged in 135 × 129 grid points which include rainfall records from 6955 rain gauge stations over India. To analyse the circulation features and moisture transport associated with the summer monsoon, the zonal (u) and meridional (v) wind components and specific humidity at 850 hPa level are used [60,61]. The wind components were collected from the European Centre for Medium-Range Weather Forecasts (ECMWF) reanalysis dataset. This ECMWF data product is based on the integrated forecasting system Cy41r2 and includes hourly output, available at a horizontal resolution of 31 km [62].

2.2. Data Analysis

All the datasets were resampled to a 0.05° × 0.05° grid using the nearest neighbour method after being processed to a monthly scale for June, July, August and September. The SST indices were derived for the WIO, NIO, CIO and the difference between the Western and Central India Ocean (W-CIO) by taking area averages over those domains. The wind speed was calculated using the formula.

Wind speed = $\sqrt{u^2 + v^2}$, where u and v are the zonal and meridional components of the wind, respectively [63].

An outline of the methodology adopted in this study is provided in Figure 2. The 18-year climatology was generated for SIF, SST, specific humidity, rainfall, soil moisture, air temperature and wind speed for June, July, August and September.

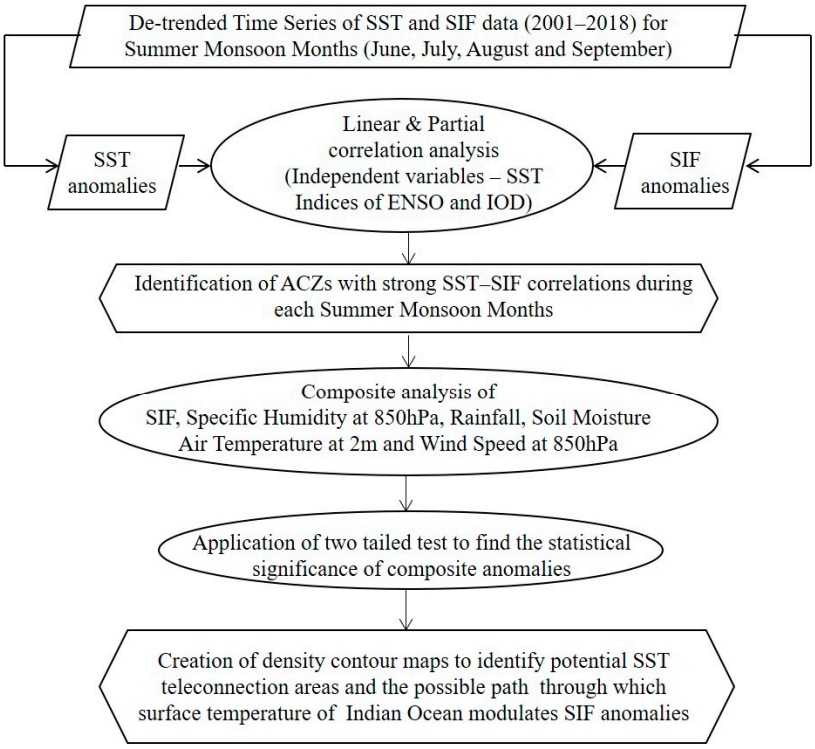

Figure 2. Methodology Flow Diagram with various steps followed for establishing the relationship between oceanic climate and terrestrial photosynthesis in the study area.

Anomalies are calculated as departures from the long-term average. Here, an anomaly time series was created for each variable at a monthly scale as $A_i = X_i - \overline{X}$, where X_i is the actual mean monthly value of the data point at ith time series and $\overline{X}$ is the monthly climatology of the variable during the period of study (2001–2018). Detrended data means the data after removing the linear trend present in the data. Time series datasets may contain trends that result in a varying mean over time. The trend is the overall change over time, but the present study deals with variability. The variability is the remaining data in

a given data span after the trend has been eliminated. Hence, excluding the trend from the time series is essential in order to capture the variability. Each monthly anomaly time series is de-trended using the first difference method, where the value at the current time step is estimated as the difference between the actual value and the value at the previous time step ($y_t' = y_t - y_{t-1}$). A de-trended time series was generated for the SST anomalies in each of the three demarcated regions in the Indian Ocean and the SIF anomalies of the 14 ACZs separately. To capture the interactions related to the climate events (ENSO and IOD), the de-trended time series of the NINO3 index and DMI were incorporated into the analysis. In addition, we calculated the difference between SST averaged for the regions of WIO and CIO (W-CIO) used in this study at a monthly scale as W-CIO = $SST_{WIO} - SST_{CIO}$.

The Pearson correlation coefficient was determined for all the region's average SST and SIF anomaly combinations to understand SST-SIF relationships' spatial and temporal variability during the summer monsoon months. To exclude the influence of concurrent ENSO and IOD events that may intrude into the direct relationship between the Indian Ocean and Indian vegetation, a partial correlation between the SST anomalies in the tropical Indian Ocean and the SIF anomalies in the ACZs was calculated by taking DMI and NINO3 index as independent variables.

Moreover, a lagged correlation between the NINO3 index and SIF anomalies was estimated to understand the delayed influence of ENSO on Indian vegetation. All the combinations of SST-SIF correlations were tested for statistical significance at 95% confidence level. Composite anomalies of SIF, specific humidity, rainfall, soil moisture, air temperature and wind speed were made for the years in which the SST variability of the tropical Indian Ocean regions fell above (below) the standard deviation of the SST anomalies observed during the period of study (2001–2018). All the composite anomalies were tested for statistical significance at a confidence level of 95% using the two-tailed Student's *t*-test, which is the most commonly accepted level of significance ($\alpha = 0.05$) considered in climate studies [64]. We incorporated only the statistically significant values in the composite anomalies and masked out others (shown in white). To identify potential SST teleconnection areas and the possible path through which the surface temperature of the tropical Indian Ocean modulates SIF anomalies across India, filled contour plots of two-dimensional scaled density estimates were generated for each of the composite anomaly maps. The scaled density estimate ranges from 0 to 1, and it is a unitless quantity.

All the frequently used abbreviations are listed in Table 2.

Table 2. List of abbreviations.

SST	Sea Surface Temperature
SIF	Solar-Induced Chlorophyll Fluorescence
WIO	Western Indian Ocean
NIO	Northern Indian Ocean
CIO	Central Indian Ocean
ENSO	El Niño Southern Oscillation
IOD	Indian Ocean dipole
DMI	Dipole mode index
ACZ	Agro-climatic zones
WCPG	Western coastal plains and Ghats
ECPH	Eastern coastal plains and hills
EPH	Eastern plateau and hills
WPH	Western plateau and hills
SPH	Southern plateau and hills

Table 2. *Cont.*

CPH	Central plateau and hills
TGP	Trans-Gangetic plains
UGP	Upper Gangetic plains
MGP	Middle Gangetic plains
LGP	Lower Gangetic plains
GPH	Gujarat plain and hills
WDR	Western dry region
WHR	Western Himalaya region
EHR	Eastern Himalaya region

3. Results

3.1. SIF and SST Variations during the Summer Monsoon

The 18-year climatology of SIF demonstrated spatial variability up to 0.55 W m^{-2} μm^{-1} sr^{-1} in the summer monsoon over India (Figure 1 and Table 3).

Table 3. Minimum, mean and maximum SIF values in each of the agro-climatic zone during the summer monsoon.

ACZ	Minimum	Mean	Maximum
WCPG	0.019	0.30	0.41
ECPH	0.011	0.20	0.47
EPH	0.013	0.25	0.45
WPH	0.013	0.18	0.38
SPH	0.016	0.17	0.41
CPH	0.01	0.17	0.34
TGP	0.01	0.18	0.34
UGP	0.049	0.22	0.37
MGP	0.014	0.22	0.43
LGP	0.022	0.24	0.41
GPH	0	0.13	0.35
WDR	0	0.05	0.19
WHR	0	0.08	0.39
EHR	0	0.35	0.54

The EHR dominated by thick forests emerged as the most productive ACZ with a mean SIF of 0.35 W m^{-2} μm^{-1} sr^{-1}, while WDR characterised by sparse vegetation and arid climate turned the least productive area having the weakest SIF signals (0.05 W m^{-2} μm^{-1} sr^{-1}). SIF depicted maximum photosynthesis during August (0.26 W m^{-2} μm^{-1} sr^{-1}) and minimum during June (0.13 W m^{-2} μm^{-1} sr^{-1}) (Figure 3). During the monsoon's initial stages, the maximum SIF values are for forest areas with a mean value of 0.20 W m^{-2} μm^{-1} sr^{-1}, while they are comparatively low over croplands (0.09 W m^{-2} μm^{-1} sr^{-1}). The contribution of the croplands to the total productivity of the vegetation in India increases rapidly (0.23 W m^{-2} μm^{-1} sr^{-1}) once the monsoon attains its peak in August. The magnitude of SIF over forest ecosystems across the country showed marginal variation in the second half of the monsoon (~0.3 W m^{-2} μm^{-1} sr^{-1}), and the SIF variability during August and September over the country is nearly the same (~0.25 W m^{-2} μm^{-1} sr^{-1}).

The tropical Indian Ocean SST exhibits a unique regional distribution during the summer monsoon. The SSTs of the Western, Northern and Central Indian Ocean (WIO, NIO and CIO) have ranges of 26.78–30.22 °C, 23.33–29.53 °C and 21.91–28.26 °C, respectively, with NIO emerging as the warmest, followed by WIO and CIO (Figure 1). The de-trended time series of mean monthly SST anomalies during the monsoon period exhibited large

interannual variability in each of the oceanic regions (Figure 4). The maximum SST anomalies were observed in WIO, followed by NIO and CIO. The SST variations in WIO, NIO and CIO seem to be considerably interlinked until 2012. After 2012, the SST fluctuations in CIO are not in phase with the SST anomalies of WIO and NIO (Figure 4a). However, the SST anomalies of WIO and NIO are consistently linked (r = +0.80) all through the period of study (Figure 4a). The time series NINO3 index, DMI and W-CIO depicted the possible influence of climate events (ENSO and IOD) on the SST variations in individual Indian Ocean regions (Figure 4b). Overall, the W-CIO index (r = +0.74), SST variability in WIO (r = +0.59) and NIO (r = +0.58) exhibited robust correlation with DMI during the period of study. Meanwhile, SST anomalies in both WIO and NIO do not closely follow the pattern of DMI during 2006–2011. Relatively, the degree of correlation between SST anomalies in the three selected Indian Ocean regions and the NINO3 index appears weaker.

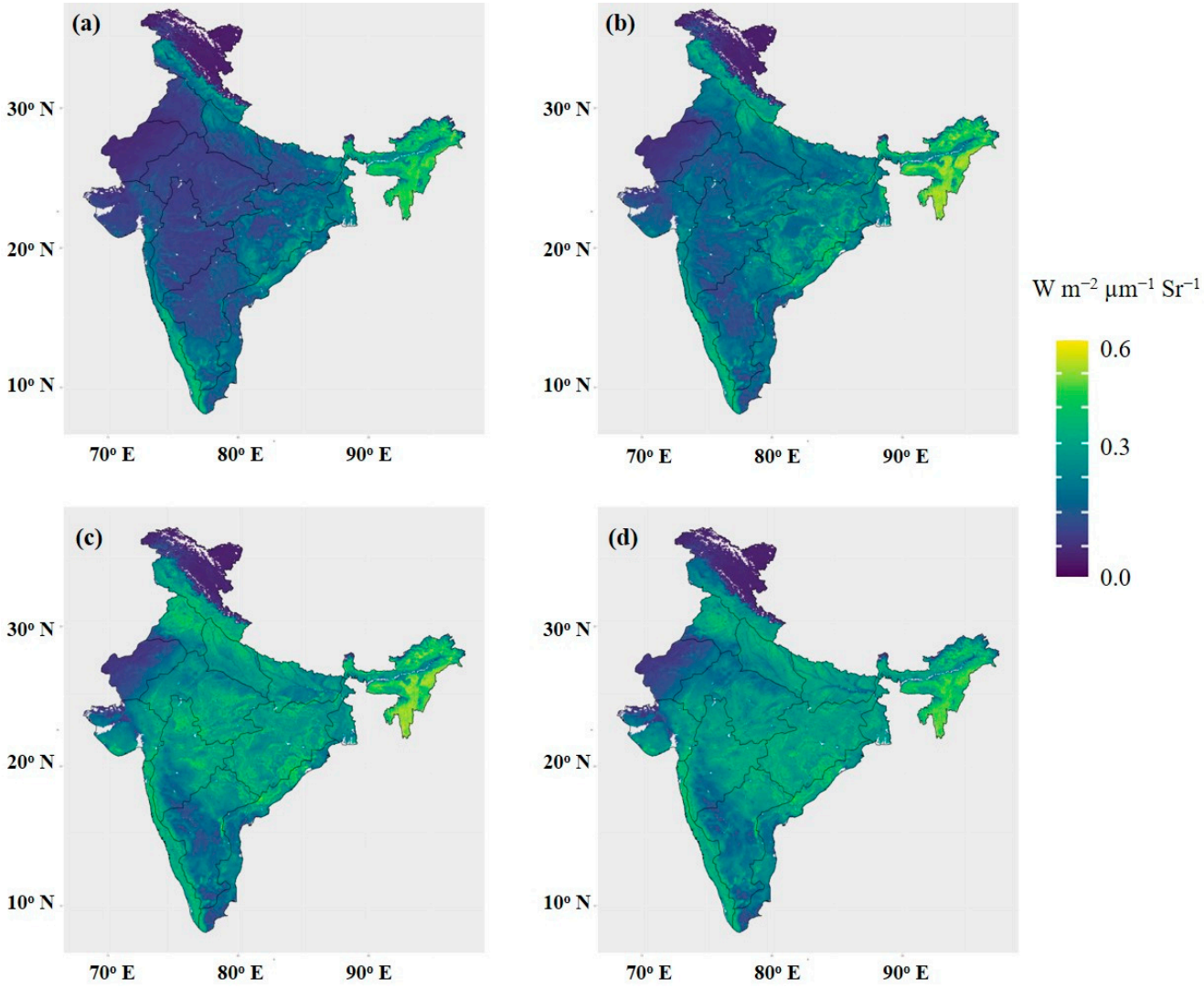

Figure 3. Spatial variation of mean SIF across India during the months of (**a**) June, (**b**) July, (**c**) August and (**d**) September indicates a progressive increase from June to September with respect to the growing season. (Software used: R version 4.0.5 (2021), https://www.R-project.org/ (accessed on 25 July 2021)).

3.2. Linear Correlations between SST and SIF

The strengths of the SST–SIF associations vary both spatially and temporally for June, July, August and September (Table 4).

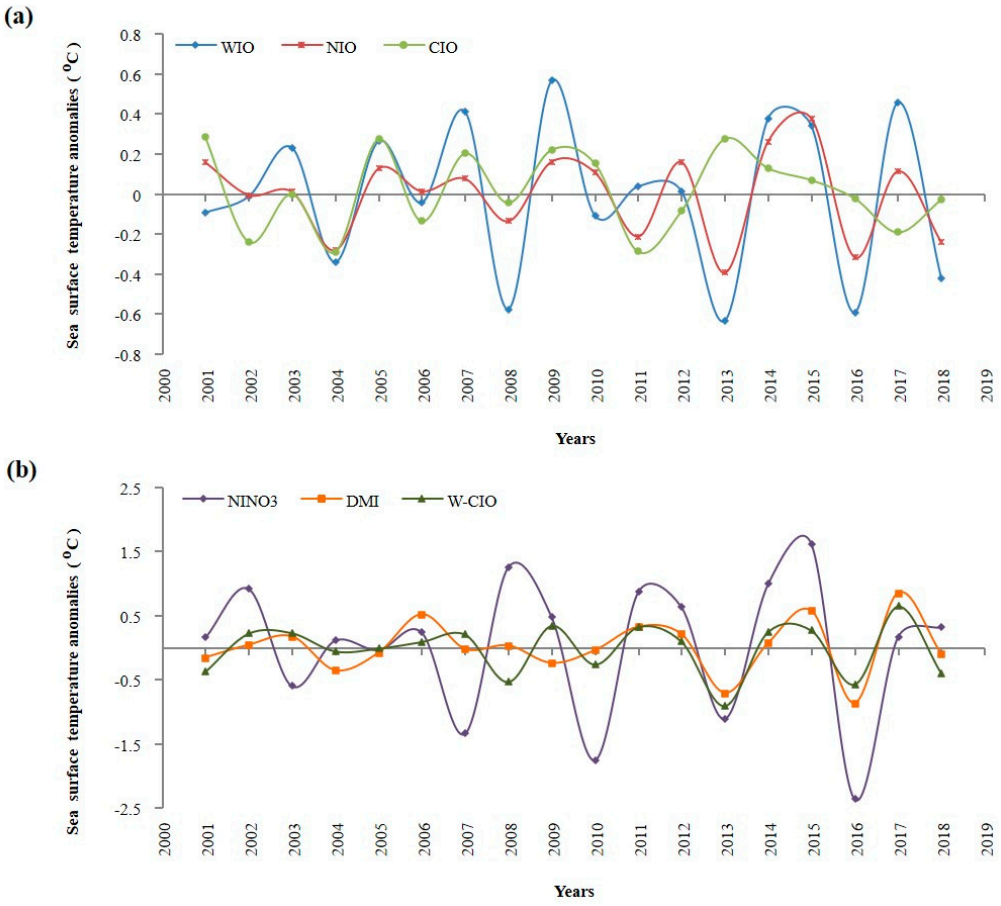

Figure 4. Time series of basin-wise average SST anomalies over (**a**) Western Indian Ocean, North Indian Ocean and Central Indian Ocean and time series of (**b**) NINO3 SST anomalies, DMI and W-CIO index during monsoon season (2001–2018), which depicts a strong interannual variability. (Software used: Python version 3.7 (2019), https://www.python.org/ (accessed on 12 September 2021) and R version 4.0.5 (2021), https://www.R-project.org/ (accessed on 12 September 2021)).

Table 4. The correlation coefficients (r) between SST and SIF during the months of June, July, August and September as mentioned across the Western, Northern and Central Indian Ocean. The correlation coefficients (r) shown in bold text are statistically significant at 95% CI.

Agro Climatic Zone	Correlation Coefficient (r)											
	Western Indian Ocean (WIO)				Northern Indian Ocean (NIO)				Central Indian Ocean (CIO)			
	Jun	Jul	Aug	Sep	Jun	Jul	Aug	Sep	Jun	Jul	Aug	Sep
WCPG	−0.4	−0.066	**+0.581**	**+0.593**	−0.083	−0.051	**+0.649**	**+0.495**	−0.296	−0.375	−0.045	+0.398
ECPH	**−0.549**	−0.142	+0.062	+0.216	−0.196	−0.077	+0.201	+0.262	−0.227	+0.147	+0.292	**+0.533**
EPH	**−0.609**	−0.207	+0.125	+0.042	**−0.534**	−0.313	+0.205	+0.141	**−0.676**	−0.241	+0.084	**+0.475**
WPH	−0.222	+0.187	−0.041	−0.332	−0.325	+0.061	+0.011	−0.270	**−0.657**	+0.266	+0.394	−0.061
SPH	**−0.478**	+0.005	−0.159	+0.037	−0.245	+0.0003	−0.037	+0.145	−0.295	+0.262	+0.317	+0.387
CPH	**−0.546**	−0.122	+0.005	−0.337	**−0.607**	−0.166	+0.163	−0.177	**−0.738**	+0.151	+0.425	+0.008
TGP	**−0.559**	−0.220	−0.368	**−0.472**	**−0.476**	−0.167	−0.184	−0.141	**−0.494**	+0.210	+0.382	+0.129
UGP	**−0.593**	−0.342	−0.115	−0.087	**−0.540**	−0.343	+0.071	−0.328	**−0.546**	−0.017	+0.116	−0.120
MGP	−0.443	−0.401	−0.201	+0.219	**−0.557**	−0.407	−0.016	+0.288	**−0.554**	−0.133	−0.290	+0.280
LGP	−0.322	−0.445	**−0.481**	−0.388	−0.282	−0.372	−0.109	+0.090	−0.317	−0.016	−0.267	+0.351
GPH	−0.291	+0.119	−0.365	−0.433	−0.387	+0.036	−0.137	−0.104	**−0.607**	+0.191	**+0.592**	+0.376
WDR	−0.408	+0.181	−0.280	**−0.512**	−0.396	+0.122	−0.031	−0.149	−0.412	+0.228	**+0.505**	+0.270
WHR	**−0.526**	−0.400	−0.095	+0.057	**−0.501**	−0.381	+0.391	+0.206	**−0.536**	−0.029	+0.453	+0.258
EHR	−0.177	−0.063	−0.369	−0.449	−0.374	−0.121	−0.229	−0.383	−0.128	+0.277	+0.227	−0.057

Overall, the Pearson correlation coefficient reached a maximum value of −0.74 between CIO and CPH in June. Only the robust SST–SIF correlations, which are statistically significant ($p < 0.05$), were considered here. The bolded values for $p < 0.05$ do not account for multiple testing. Broadly, the SIF anomalies of all the ACZs except EHR appear to be impacted by SST variations in at least one tropical Indian Ocean region during one of the monsoon months. The SST anomalies for June in WIO showed statistically significant correlations with the SIF variability of ECPH (−0.55), EPH (−0.61), SPH (−0.48), CPH (−0.55), TGP (−0.56), UGP (−0.59) and WHR (−0.53), while the correlations with the SIF variability in August in WCPG and LGP were +0.58 and −0.48, respectively. For the month of September, WIO exhibited a significant correlation with WCPG (+0.59), TGP (−0.47) and WDR (−0.51). The SST anomalies in NIO also displayed a considerable degree of correlation with the SIF anomalies of EPH (−0.53), CPH (−0.61), MGP (−0.56), UGP (−0.54), TGP (−0.48) and WHR (−0.50) in June. Considerable SST–SIF links were observed only between NIO and WCPG in August (+0.65) and September (+0.50). Similarly, at the onset of the monsoon, the CIO SST anomalies were linked to the SIF anomalies of EPH (−0.68), WPH (−0.66), CPH (−0.74), TGP (−0.50), UGP (−0.55), MGP (−0.55), GPH (−0.60) and WHR (−0.54). These ACZs cover the entire Deccan Plateau except for the southern parts, the full stretch of the Indo-Gangetic Plains and India's hot and cold deserts. When the monsoon peaks in August, the teleconnections with the CIO SST anomalies were confined to the arid regions of GPH (+0.59) and WDR (+0.51) on the western Indian boundary. CIO SST influence shifted to ECPH (+0.53) and EPH (+0.48) of eastern coastal India, corresponding to monsoon withdrawal. However, the significant SST-SIF correlations observed after June were very limited.

3.3. Partialling out of ENSO and IOD Teleconnections from SST-SIF Correlations

To avoid interferences from the ENSO and IOD events, we calculated the partial correlation among the selected SST–SIF relationships and only statistically significant correlations are discussed here (Table 5). All the highlighted ACZs maintained the link with the tropical Indian Ocean regions. Even after excluding the influences of ENSO and IOD, the degree of the SST-SIF association did not diminish greatly compared to the standard linear correlations (Table 4), and most of those relationships remained statistically significant. The intensity of the ENSO and IOD effects on the SIF variability across India was found to be less in June, but it increased as the monsoon proceeded. Even with the removal of NINO3 SST effects and the DMI from the respective months, most of the ACZs across the northern and central-eastern portions of India maintained their relationship with WIO during the monsoon onset period. Similarly, the significance of the NIO and CIO SST anomalies is still considerable in all of the selected ACZs. No considerable correlation was observed among WIO SST and SIF anomalies after June. As the monsoon peaks in August, NIO showed significant connections only with WCPG, and CIO exhibited links with GPH and WDR. During September, the linkage of the CIO SST with the SIF anomalies of ECPH and EPH was maintained. However, many SST-SIF correlations discovered after June become insignificant after removing ENSO or IOD effects (Table 5). However, certain ambiguities may still exist in the reported SST–SIF correlations. On the other hand, the composite of SIF anomalies illustrates how India's terrestrial photosynthetic activity specifically responds to the anomalous positive and negative SST years in the Western, Northern and Central Indian Oceans. This would clearly represent the impact of the tropical Indian Ocean SST variability on the Indian vegetation anomalies.

3.4. The SST–SIF Link during the Onset Phase of Summer Monsoon

The inverse ocean-land linkage observed in the correlation analyses was also found in the composite anomalies of SIF (Figure 5). The years selected to make the composite anomalies are given in Table S1. The linkage between Indian vegetation SIF anomalies and the tropical Indian Ocean SST was verified using composite anomalies of the important hydroclimatic variables (specific humidity, rainfall, soil moisture and air temperature).

These auxiliary parameters depict how the SST variations in WIO, NIO and CIO are connected with the SIF anomalies through modulation of the water available to the plants for photosynthesis over India.

Table 5. Partial Correlation coefficient was determined to understand the independent influence of SST fluctuations in Indian Ocean basins over the months of June, August and September, where SST anomalies due to ENSO and IOD events were kept as fixed variables. The highlighted Agro-climatic zones contain the impact of climatic oscillations in the observed SST-SIF relationship. The correlation coefficients (r) shown in bold text are statistically significant at 95% CI.

Oceanic Region	Partial Correlation Coefficient (r) between Indian Ocean SST and SIF Limiting NINO3 Index and DMI								
	June			August			September		
	ACZ	Independent Variables		ACZ	Independent Variables		ACZ	Independent Variables	
		NINO3	DMI		NINO3	DMI		NINO3	DMI
WIO	ECPH	−0.55	−0.38	WCPG	+0.51	+0.16	WCPG	+0.58	+0.316
	EPH	**−0.63**	**−0.56**	LGP	−0.59	−0.32	TGP	−0.37	−0.69
	CPH	**−0.56**	**−0.66**				WDR	−0.34	−0.72
	SPH	−0.49	−0.37						
	TGP	**−0.57**	**−0.59**						
	UGP	**−0.62**	**−0.52**						
	WHR	**−0.55**	**−0.50**						
NIO	**EPH**	**−0.51**	**−0.49**	**WCPG**	**+0.59**	**+0.54**	WCPG	+0.46	+0.24
	CPH	**−0.58**	**−0.65**						
	TGP	**−0.45**	**−0.47**						
	UGP	**−0.51**	**−0.49**						
	MGP	**−0.52**	**−0.52**						
	WHR	**−0.46**	**−0.47**						
CIO	**EPH**	**−0.66**	**−0.72**	**GPH**	**+0.55**	**+0.58**	**ECPH**	**+0.55**	**+0.48**
	WPH	**−0.65**	**−0.66**	**WDR**	**+0.46**	**+0.53**	**EPH**	**+0.53**	**+0.48**
	CPH	**−0.72**	**−0.74**						
	TGP	**−0.46**	**−0.50**						
	UGP	**−0.51**	**−0.59**						
	MGP	**−0.52**	**−0.58**						
	GPH	**−0.58**	**−0.61**						
	WHR	**−0.50**	**−0.56**						

The density contours of SIF anomalies showed that the regions over the Indian mainland with a significant impact on tropical Indian Ocean SST variability. Notable negative SIF anomalies are observed in central and northern India when the WIO, NIO and CIO are warmer-than-normal (Figure 5a–c). Similarly, the influence of colder-than-normal surface waters in the same oceanic regions enhances plants' photosynthetic rates in some ecosystems, as displayed by the density contour of positive SIF anomalies (Figure 5d–f). However, a considerable bias exists between the influence of warm and cold SST anomalies on the SIF anomalies over India. The impact of warm SST anomalies appears more profound than cold anomalies in the tropical Indian Ocean. However, apart from the results obtained in the correlation analysis, some other ACZs were also influenced by SST variations in the WIO. This predominantly includes MGP and WPH, particularly when warm SST anomalies persist in the WIO. Overall, the effect of WIO warm anomaly concentrated mainly on the SIF anomalies of WHR, TGP, UGP, MGP, EPH, WPH and CPH (Figure 5a). At the same time, the influence of negative SST anomalies in the WIO focused mainly on EPH and CPH (Figure 5d). The impact of NIO's SST is confined to the ACZs that lie in the north-central areas. As per the SST–SIF correlations, the NIO governs the SIF anomalies in the EPH, CPH, WHR, TGP, UGP and MGP. The density contour plots also reveal the same results during the years of warm anomalies in the NIO (Figure 5b). However, the oceanic influence from NIO lies predominantly over SIF anomalies in CPH during cold anomaly years (Figure 5e). The SST patterns in the western and central oceanic regions are nearly identical (Figure 1). This similarity is almost observed in the SST teleconnections to SIF anomalies over India.

The influence of CIO was predominantly observed in the Indo-Gangetic Plains and the northern and central regions of India (Figure 5c,f). As with the SST interactions from WIO, the SST anomalies in CIO govern the vegetation photosynthesis of EPH, CPH, UGP, TGP and WHR. Furthermore, GPH, WPH and MGP also showed linkages with CIO (Table 5). Contrary, GPH failed to exhibit significant linkage with CIO SST anomalies, as depicted in the density contours of SIF anomalies. At the same time, SIF anomalies in the WDR were found to be closely associated with positive SST anomalies in the CIO (Figure 5c).

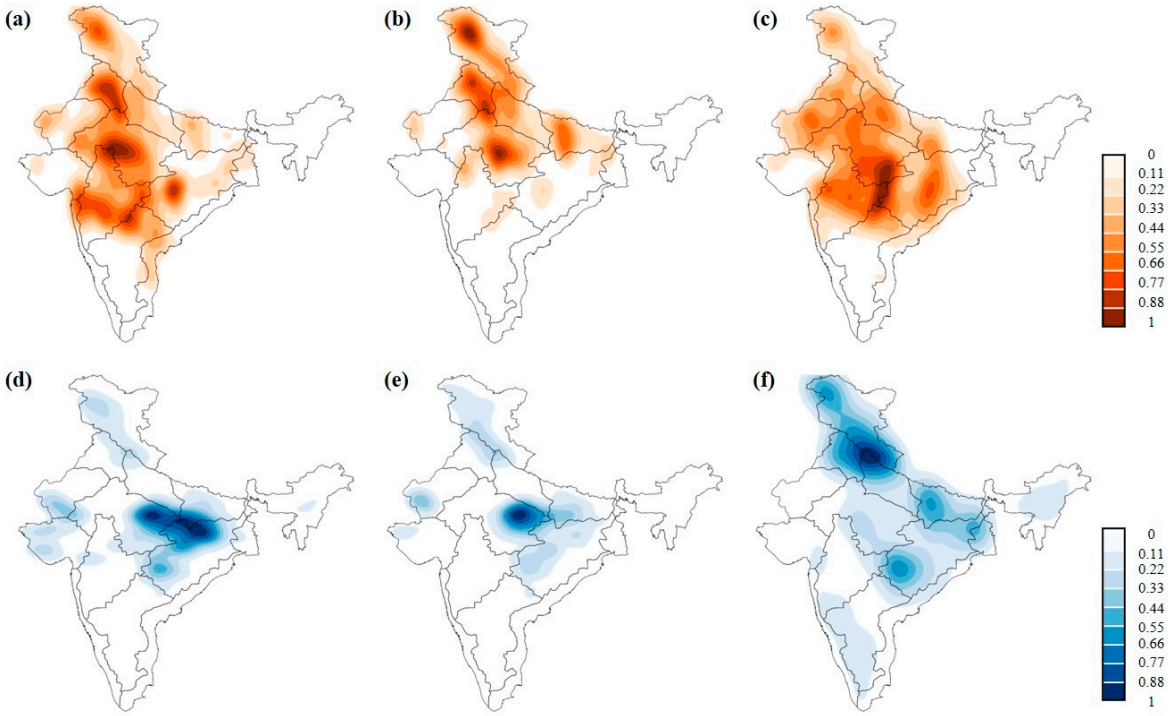

Figure 5. Regions showing statistically significant composite anomalies of SIF (W m^{-2} μm^{-1} Sr^{-1}) across India during the month of June when SST anomalies of the Western Indian Ocean (**a**,**d**), Northern Indian Ocean (**b**,**e**) and Central Indian Ocean (**c**,**f**) demonstrated positive (upper) and negative (lower) trends. The colour bar shows the scaled density estimate of negative (orange) and positive (blue) SIF anomalies. The warmer SST in the oceanic regions leads to negative SIF anomalies, while the colder SST leads to positive SIF anomalies.

However, the composites of SIF anomalies almost agree with the observed SST-SIF correlations. During years of warmer than normal surface waters in the tropical Indian Ocean regions, negative anomalies of the specific humidity (Figure 6a–c), rainfall (Figure 7a–c), and soil moisture (Figure 8a–c) together with positive air temperature anomalies (Figure 9a–c) were dominantly observed in India. The consequent water stress condition reduces vegetation productivity and thus exhibits negative anomalies of SIF.

Similarly, negative anomalies of air temperature (Figure 9d–f), together with positive anomalies of specific humidity (Figure 6d–f), rainfall (Figure 7d–f) and soil moisture (Figure 8d–f), occur corresponding to the negative SST anomalies in WIO, NIO and CIO. This reduces the chances of the vegetation experiencing water stress and thus exhibits positive SIF anomalies. The bias exists in the implications of warm and cold SST anomalies are clearly evident in the density plots of specific humidity, rainfall, soil moisture and air temperature anomalies. However, the agro-meteorological metrics studied here show corresponding anomalies that almost match the SIF pattern on the same terrestrial band. Overall, the results suggest that the relationship between SST variations in the Western, Northern and Central Indian Ocean and SIF anomalies across India is feasible through atmospheric teleconnections during June.

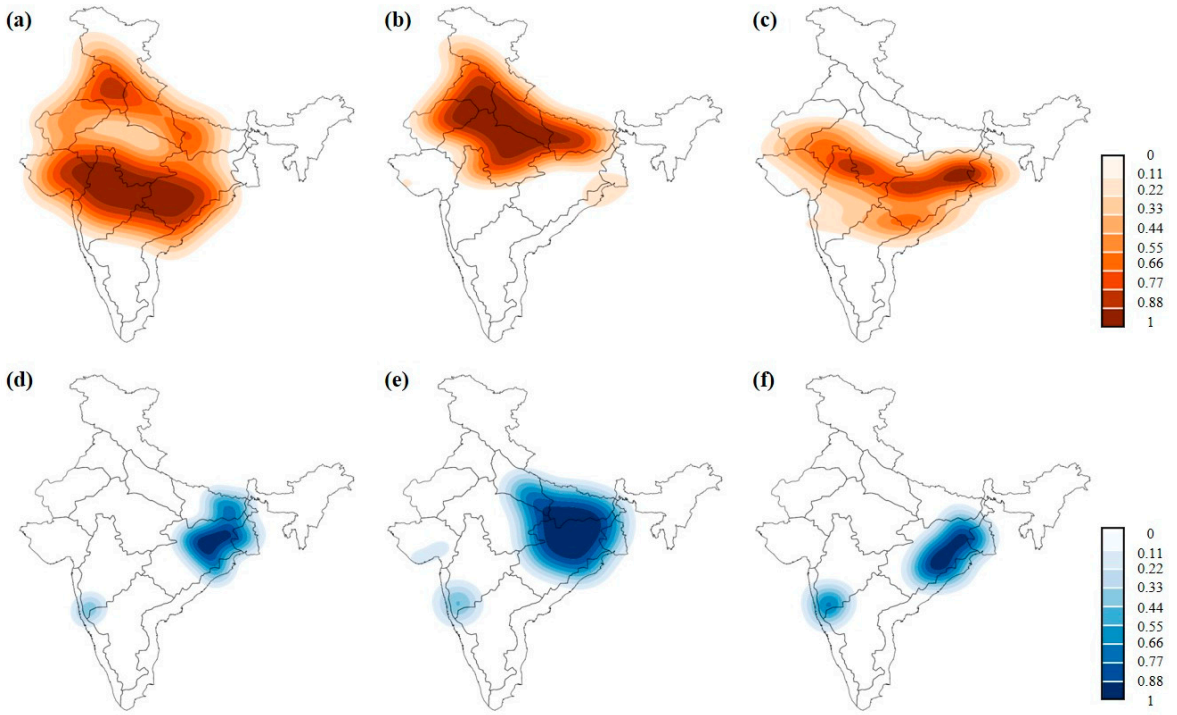

Figure 6. Regions showing statistically significant composite anomalies of specific humidity (kg/kg) across India during the month of June when SST anomalies of the Western Indian Ocean (**a**,**d**), Northern Indian Ocean (**b**,**e**) and Central Indian Ocean (**c**,**f**) demonstrated positive (upper) and negative (lower) variations. The colour bar shows the scaled density estimate of negative (orange) and positive (blue) specific humidity anomalies. The warmer SST in the oceanic regions leads to negative specific humidity anomalies, while the colder SST leads to positive specific humidity anomalies in the shaded areas. (Software used: Python version 3.7 (2019), https://www.python.org/ (accessed on 8 November 2021) and R version 4.0.5 (2021), https://www.R-project.org/ (accessed on 6 November 2021)).

There also exist slight deviations in the cause-effect chain of identified SST-SIF links. This is most notable in the WHR, where no significant anomalies were observed in the hydroclimatic variables similar to the SIF pattern. However, the positive and negative SIF anomalies observed mainly over the central and northern parts of India during the years of negative and positive SST anomalies, respectively, in the tropical Indian Ocean, appear justifiable based on the observed anomalies of hydroclimate variables.

3.5. The SST–SIF Link after the Onset of the Summer Monsoon

The characteristic inverse tropical Indian Ocean SST influence on SIF anomalies weakens considerably over the Indian mainland after June. Overall, the association between SST anomalies of the individual Indian Ocean regions and SIF anomalies across India seems to weaken after the monsoon onset (Table 5). Meanwhile, mostly statistically significant positive SST–SIF associations were observed once the monsoon establishes across the country. The composite of SIF anomalies also demonstrated these varying responses of vegetation photosynthetic activity to the tropical Indian Ocean SSTs (Figures S1–S3). The well-defined patterns of negative SST-SIF relations discovered during the onset phase of the monsoon (Figure 5) then appeared as a mixed and irregular relationship in July (Figure S1), August (Figure S2) and September (Figure S3). However, in July, notable positive SIF anomalies were observed across SPH, WPH, GPH and WDR as a result of warm SST anomalies in WIO (Figure S1a). In contrast, considerable negative SIF anomalies in the same region are found only when cold SST anomalies persist mainly in the CIO region (Figure S1f). In August, positive and negative SIF anomalies concentrated across WDR in response to the positive and negative SST anomalies in the CIO, respectively (Figure S2c,f). As the

monsoon withdraws in September, SIF anomalies over India failed to vary in relation to the SST anomalies in WIO, NIO and CIO (Figure S3). However, the cause–effect chain of SST and SIF was found to be weak in July (Figure S4i–iv), August (Figure S5i–iv) and September (Figure S6i–iv), and the observed composite anomalies did not complement each other. This points to the complexity of the physical processes associated with each phase of the summer monsoon.

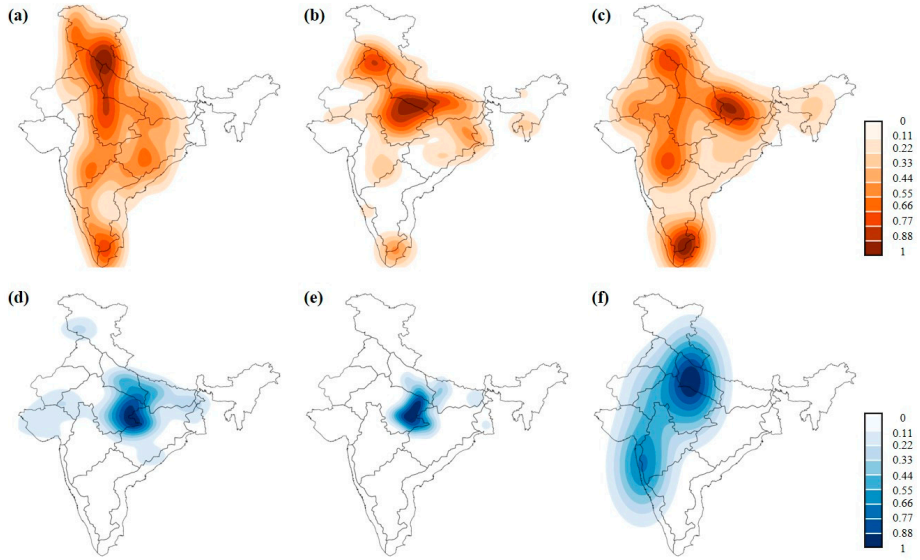

Figure 7. Regions showing statistically significant composite anomalies of rainfall (mm) across India during the month of June when SST anomalies of the Western Indian Ocean (**a**,**d**), Northern Indian Ocean (**b**,**e**) and Central Indian Ocean (**c**,**f**) demonstrated positive (upper) and negative (lower) variations. The colour bar shows the scaled density estimate of negative (orange) and positive (blue) rainfall anomalies. The warmer SST in the oceanic regions leads to negative rainfall anomalies, while the colder SST leads to positive rainfall anomalies in the shaded areas.

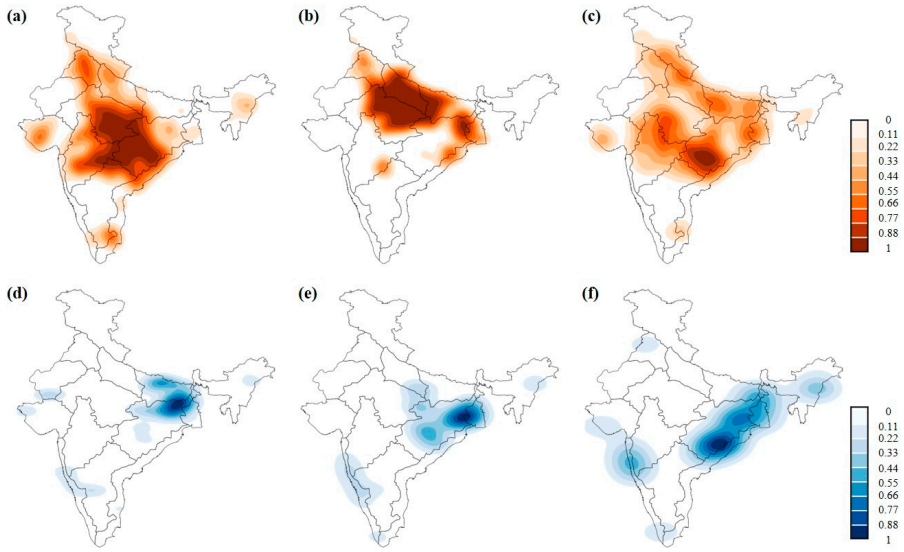

Figure 8. Regions showing statistically significant composite anomalies of soil moisture (m^3/m^3) across India during the month of June when SST anomalies of the Western Indian Ocean (**a**,**d**), Northern Indian Ocean (**b**,**e**) and Central Indian Ocean (**c**,**f**) demonstrated positive (upper) and negative (lower) variations. The colour bar shows the scaled density estimate of negative (orange) and positive (blue) soil moisture anomalies. The warmer SST in the oceanic regions leads to negative soil moisture anomalies, while the colder SST leads to positive soil moisture anomalies in the shaded areas.

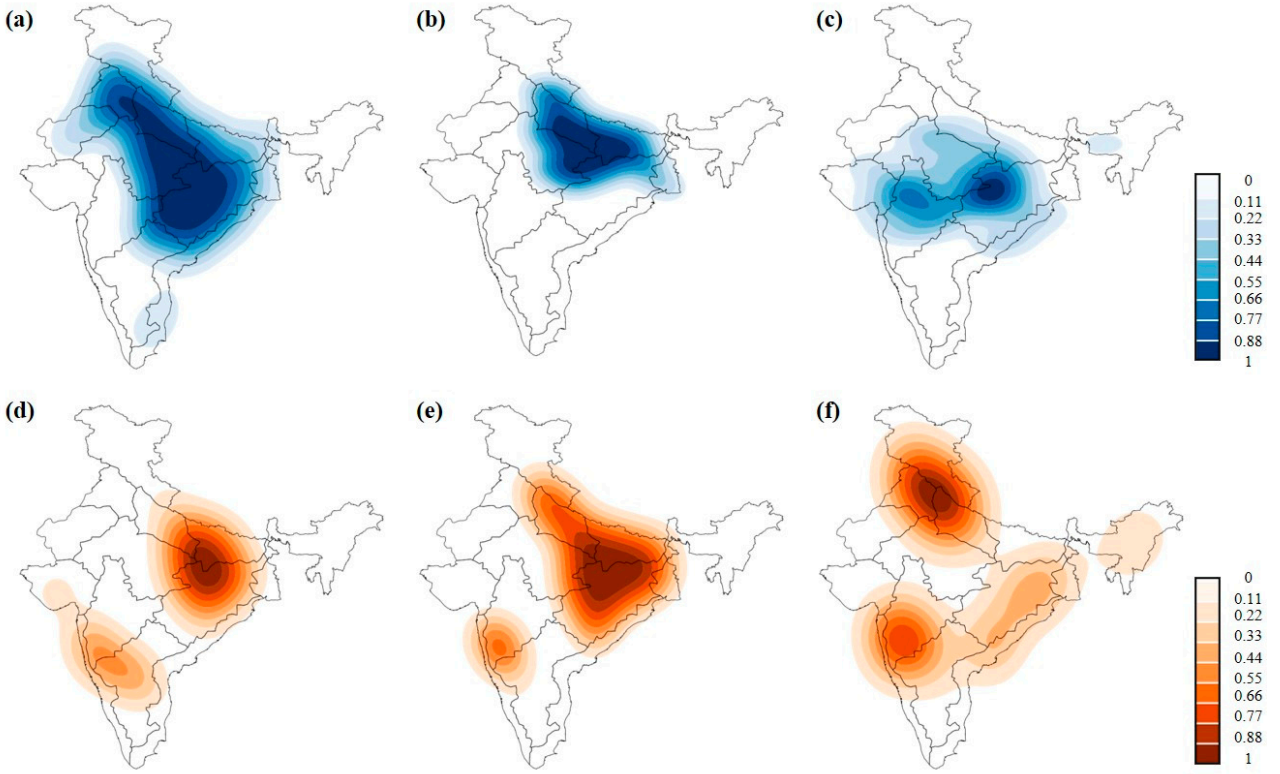

Figure 9. Regions showing statistically significant composite anomalies of air temperature (°C) across India during the month of June when SST anomalies of the Western Indian Ocean (**a**,**d**), Northern Indian Ocean (**b**,**e**) and Central Indian Ocean (**c**,**f**) demonstrated positive (upper) and negative (lower) variations. The colour bar shows the scaled density estimate of positive (blue) and negative (orange) air temperature anomalies. The warmer SST in the oceanic regions leads to positive air temperature anomalies, while the colder SST leads to negative air temperature anomalies in the shaded areas.

4. Discussion

The SST has a significant impact on air-sea interactions and drives global weather systems and climate patterns. Therefore, changes in the SST, either increase or decrease, can cause a wide variety of impacts on every component of the climate system. The vegetation dynamics across India mainly depend on seasonally occurring rainfall events, especially in the summer monsoon, which is also linked to the regional SST variations in the Indian Ocean [65,66]. Therefore, it is expected that the vegetation anomalies in India are linked to the SST variability in the Indian Ocean. This is correct on a seasonal scale, and we investigated the details by stratifying the monsoon season into individual months (June, July, August and September). Moreover, there is a significant intraseasonal oscillation in this SIF pattern, which corresponds to the intraseasonal variability of vegetation photosynthesis during different summer monsoon phases. Predominantly, the ACZs in the Indo-Gangetic Plains and the central Indian region displayed notable variability in SIF due to significant intraseasonal variations in the monsoon rainfall at these locations [66,67]. The idea behind the stratified analysis was to understand the intra-seasonal variability of the SST–SIF relationship rather than establish a general relationship for a season. Indeed, as expected, a significant SST–SIF link was found between the tropical Indian Ocean and Indian vegetation photosynthetic activity in the monsoon onset period. During the initial phase of the summer monsoon, the Indian Ocean acts as the dominant moisture source over the Indian subcontinent, which appears to be the prime reason for observing significant SST-SIF correlations during the summer monsoon onset period. As the monsoon progresses, terrestrial sources become the prominent contributors to atmospheric moisture [68]. Therefore, the rest of this discussion is mostly based on the June SST–SIF relationship. Our findings give another dimension to the impact of climate on the Indian terrestrial

ecosystem by incorporating teleconnections stemming from SST variations in the tropical Indian Ocean.

4.1. The Possible Physical Mechanisms behind the Significant SST–SIF Relationships during the Onset Phase of the Monsoon

The inverse nature of the SST–SIF relationship in June indicates that photosynthesis anomalies over the Indian mainland react opposite to SST anomalies in the Indian Ocean regions during the onset phase of the summer monsoon. The persistence of warmer SST anomalies in the tropical Indian Ocean weakens the monsoon circulation, possibly by reducing the land–sea thermal gradient and thus suppresses the rainfall across north and central Indian regions [69]. The weak southwesterly wind is also evident in the composite anomalies of wind speed vectors over the entire study area (Figure S7a–c), and it hinders the moisture transport from the tropical Indian Ocean, as depicted by northeasterly anomalies. The consequent reduction in rainfall and soil moisture and the increase in air temperature create water stress in plants and dampen the photosynthetic activity [70–72], which led to the negative anomaly of SIF in central and northern India. Similarly, cold SST anomalies in the Indian Ocean help to maintain a strong monsoon circulation. The relatively strong summer monsoon winds blowing from the southwest of the tropical Indian Ocean region (Figure S7d–f) bring ample water to India. The resultant positive rainfall anomalies generate positive anomalies of soil moisture, reduce the chances of water stress together with cooler air temperature anomalies and, therefore, result in positive anomalies of SIF. Meanwhile, we do not rule out the possibility of reduced rainfall over the central and northern Indian regions in June due to the late onset or late progress of monsoon as a result of positive SST anomalies in the Indian Ocean [73]. This condition can also dampen the photosynthetic activity and produce negative SIF anomalies in India. The SST variations in Niño regions may have influenced SST anomalies of the tropical Indian Ocean in June. However, the rainfall anomalies in India are directly linked to the SST conditions in the tropical Indian Ocean, and the contribution of tropical Indian Ocean SST to the monsoon variability appears more dominant than the Niño SSTs, at least during the onset phase [73]. The observed SIF anomalies in India showed a good degree of coupling with tropical Indian Ocean SST variability. Meanwhile, NINO3 SST anomalies failed to exhibit considerable correlations with SIF anomalies in June, even after considering a time lag of 5 months (Figure S8). Furthermore, the study focuses exclusively on the relationship between SST anomalies in the tropical Indian Ocean regions and SIF anomalies in India and not on the factors contributing to tropical Indian Ocean SST and the monsoon variability in India. The identified ocean-vegetation linkage may be useful to track the vegetation growth anomalies in India concerning the tropical Indian Ocean SST variability.

Overall, the local tropical Indian Ocean SST effect was observed mostly in the SIF anomalies across the central and northern Indian regions, where the land largely comprises rain-fed agricultural lands and forest ecosystems, the productivity of which fluctuates according to the monsoon rainfall [33,74]. Mostly an arid–semi-arid climatic condition persists in the ACZs of this region and, in some areas, shifts to sub-humid climates. Normally, the hydrologic fluctuations control vegetation photosynthesis in arid to semi-arid ecosystems [75,76], and the net primary productivity of the forest ecosystems in the tropical belt depends on precipitation to a large extent [77].

The Indian Ocean is warming in response to global warming, and the impact of this warming through atmospheric teleconnections should reflect on the functional characteristics of terrestrial vegetation. An attempt is made to infer such a possibility on the basis of the present analyses though no attempt has been made here to understand the influence of the Indian Ocean warming trend. It was found that the warmer years of the Indian Ocean are more influential as compared with the cooler years, indicating a bias of the SST–SIF link to warmer trends. This means a warmer Indian Ocean condition may lead to reduced terrestrial photosynthetic activity in India in the initial phase of the monsoon

period. Consequently, the decline in photosynthetic carbon uptake would gradually alter the land–atmosphere interactions and affect the climate over the Indian subcontinent.

4.2. Weakening of the SST–SIF Relationship after the Onset Phase of Monsoon

The significant inverse influence of tropical Indian Ocean SST observed on the Indian vegetation in June appears to deteriorate thereafter. Even though the SIF anomalies mostly exhibit a positive linkage with the SST anomalies in the tropical Indian Ocean regions during July, August and September, their intensities, as well as spatial coverage, are small and different compared with the onset phase. The corresponding SIF anomalies observed during the years of positive and negative SST anomalies in the tropical Indian Ocean seem to be extremely weak and lack specific patterns. Therefore, the variability of vegetation photosynthetic activity in India is not considerably affected by the concurrent SST anomalies in the tropical Indian Ocean after the monsoon onset phase. This may be because once the monsoon establishes over the country after June, convective heating plays an important role in maintaining the tropospheric temperature gradient and the monsoon circulation during the remaining months [65,69]. Furthermore, the recharge of soil water during the initial phase of the monsoon helps the atmospheric moisture from terrestrial sources to become more active through evapotranspiration and contributes significantly to the Indian summer monsoon [78]. Therefore, the observed decoupling of the ocean–vegetation links after the onset of the monsoon could be due to the establishment of more local circulations owing to terrestrial moisture build-ups and/or the effects of local interference.

5. Conclusions

The present study comprehensively evaluated the impact of tropical Indian Ocean SST variability on the vegetation photosynthetic activity in India during the summer monsoon. We explored the varying responses of vegetation photosynthesis in India to the SST anomalies in the tropical Indian Ocean regions during each of the summer monsoon months. We used OCO-2 satellite-based SIF data product to represent the terrestrial vegetation photosynthesis. SIF measurements act as a unique proxy of actual plant photosynthesis, which aids in the diagnosis of plant stress conditions in real-time and, therefore, can effectively indicate the vegetation growth anomalies well in advance. Our results revealed the robust negative relationship between SST variations in the tropical Indian Ocean regions and SIF anomalies over the central and northern Indian mainland during the summer monsoon onset phase. Compared to the cold anomalies in the tropical Indian Ocean, the teleconnections stemming from the warm SST anomalies are profound and more significant on the observed SIF anomalies in India. The notable Indian Ocean SST link with the SIF anomalies in India deteriorates immediately after the onset of the monsoon. Therefore, vegetation activity in India is not significantly affected by the SST variations in the tropical Indian Ocean after June.

Scope and Challenges

Our study focused exclusively on the magnitude and nature of the SST–SIF relationship to understand the contribution of the tropical Indian Ocean variability to the vegetation anomalies in India. However, other factors would influence this ocean–atmosphere–vegetation interaction, especially during the monsoon period. The observed SST-SIF relationship can be extended further by incorporating the time lag between them, which may aid in a better understanding of varying vegetation responses to SST variations in the tropical Indian Ocean. Being an agricultural-based country, human factors like improvements in irrigation infrastructure would considerably impact the variability of crop productivity in India. Incorporating these human activities might also help to better understand the mechanism behind the decreased SST link to overall Indian SIF, particularly in the months of July, August and September. An extensive study with more data and detailed analysis could be the future scope of our study. The contribution of the SST to the SIF anomalies suggests the predictability of possible outward changes in the growth and physiological

status of vegetation in India resulting from anomalous SST of the tropical Indian Ocean. Such forecasts are beneficial to forest management practices and the efficient use of water resources in croplands under extreme climate conditions. They may also contribute to the understanding of future imbalances in the Indian terrestrial carbon budget arising from climate change.

Supplementary Materials: The following supporting information can be downloaded at: https://www.mdpi.com/article/10.3390/rs15071756/s1, Table S1: Years considered for the composite anomalies during June. Figure S1: Regions showing statistically significant composite anomalies of SIF (W m^{-2} μm^{-1} Sr^{-1}) across India during the month of July when, SST anomalies of the Western Indian Ocean (a,d), Northern Indian Ocean (b,e), and Central Indian Ocean (c,f) demonstrated positive (upper) and negative (lower) trends. The warmer SST in the oceanic regions lead to positive SIF anomalies, while colder SST leads to negative SIF anomalies. Figure S2: Regions showing statistically significant composite anomalies of SIF (W m^{-2} μm^{-1} Sr^{-1}) across India during the month of August when, SST anomalies of the Western Indian Ocean (a,d), Northern Indian Ocean (b,e), and Central Indian Ocean (c,f) demonstrated positive (upper) and negative (lower) trends. The warmer SST in the oceanic regions lead to positive SIF anomalies, while colder SST leads to negative SIF anomalies. Figure S3: Regions showing statistically significant composite anomalies of SIF (W m^{-2} μm^{-1} Sr^{-1}) across India during the month of September when, SST anomalies of the Western Indian Ocean (a,d), Northern Indian Ocean (b,e), and Central Indian Ocean (c,f) demonstrated positive (upper) and negative (lower) trends. The warmer SST in the oceanic regions lead to positive SIF anomalies, while colder SST leads to negative SIF anomalies. Figure S4-i: Regions showing statistically significant composite anomalies of specific humidity (Kg/Kg) across India during the month of July when, SST anomalies of the Western Indian Ocean (a,d), Northern Indian Ocean (b,e), and Central Indian Ocean (c,f) demonstrated positive (upper) and negative (lower) variations. Figure S4-ii: Regions showing statistically significant composite anomalies of rainfall (mm) across India during the month of July when, SST anomalies of the Western Indian Ocean (a,d), Northern Indian Ocean (b,e), and Central Indian Ocean (c,f) demonstrated positive (upper) and negative (lower) variations. Figure S4-iii: Regions showing statistically significant composite anomalies of soil moisture (m^3/m^3) across India during the month of July when, SST anomalies of the Western Indian Ocean (a,d), Northern Indian Ocean (b,e), and Central Indian Ocean (c,f) demonstrated positive (upper) and negative (lower) variations. Figure S4-iv: Regions showing statistically significant composite anomalies of air temperature (°C) across India during the month of July when, SST anomalies of the Western Indian Ocean (a,d), Northern Indian Ocean (b,e), and Central Indian Ocean (c,f) demonstrated positive (upper) and negative (lower) variations. Figure S5-i: Regions showing statistically significant composite anomalies of specific humidity (Kg/Kg) across India during the month of August when, SST anomalies of the Western Indian Ocean (a,d), Northern Indian Ocean (b,e), and Central Indian Ocean (c,f) demonstrated positive (upper) and negative (lower) variations. Figure S5-ii: Regions showing statistically significant composite anomalies of rainfall (mm) across India during the month of August when, SST anomalies of the Western Indian Ocean (a,d), Northern Indian Ocean (b,e), and Central Indian Ocean (c,f) demonstrated positive (upper) and negative (lower) variations. Figure S5-iii: Regions showing statistically significant composite anomalies of soil moisture (m^3/m^3) across India during the month of August when, SST anomalies of the Western Indian Ocean (a,d), Northern Indian Ocean (b,e), and Central Indian Ocean (c,f) demonstrated positive (upper) and negative (lower) variations. Figure S5-iv: Regions showing statistically significant composite anomalies of air temperature (°C) across India during the month of August when, SST anomalies of the Western Indian Ocean (a,d), Northern Indian Ocean (b,e), and Central Indian Ocean (c,f) demonstrated positive (upper) and negative (lower) variations. Figure S6-i: Regions showing statistically significant composite anomalies of specific humidity (kg/kg) across India during the month of September when, SST anomalies of the Western Indian Ocean (a,d), Northern Indian Ocean (b,e), and Central Indian Ocean (c,f) demonstrated positive (upper) and negative (lower) variations. Figure S6-ii: Regions showing statistically significant composite anomalies of rainfall (mm) across India during the month of September when, SST anomalies of the Western Indian Ocean (a,d), Northern Indian Ocean (b,e), and Central Indian Ocean (c,f) demonstrated positive (upper) and negative (lower) variations. Figure S6-iii: Regions showing statistically significant composite anomalies of soil moisture (m^3/m^3) across India during the month of September when, SST anomalies of the Western Indian Ocean (a,d), Northern Indian Ocean (b,e), and Central Indian Ocean (c,f) demonstrated positive (upper)

and negative (lower) variations. Figure S6-iv: Regions showing statistically significant composite anomalies of air temperature (°C) across India during the month of September when, SST anomalies of the Western Indian Ocean (a,d), Northern Indian Ocean (b,e), and Central Indian Ocean (c,f) demonstrated positive (upper) and negative (lower) variations. Figure S7: Density contour plot of summer monsoon wind at 850 hPa during June when, SST anomalies of the Western Indian Ocean (a,d), Northern Indian Ocean (b,e), and Central Indian Ocean (c,f) demonstrated positive (upper) and negative (lower) variations. Colouration indicates the density estimate of wind speed anomalies, which are statistically significant and the arrows indicate the wind direction. Figure S8: Shows the correlation of SIF anomalies with NINO3 SST anomalies during June at (i) lag 0, (ii) lag 1, (iii) lag 2, (iv) lag 3, and (v) lag (iv, and (vi) lag 5. Statistically significant correlation coefficient (p-value < 0.05, r-value > 0.5) is depicted and other values are masked out. (Software used: Python version 3.7 (2019), https://www.python.org/, accessed on 20 April 2022).

Author Contributions: Conceptualization, R.V., M.D.B., and S.K.B.; Formal analysis; Methodology, R.V., M.D.B., and S.K.B.; supervision, S.K.B. and M.D.B.; Writing—original draft, R.V.; writing—review and editing, S.K.B. and M.D.B. All authors have read and agreed to the published version of the manuscript.

Funding: This research received no external funding.

Data Availability Statement: The GOSIF is available at Global Ecology Group's data repository on reasonable request (http://data.globalecology.unh.edu/ (accessed on 16 March 2021)). The OISST dataset is collected from National Centers for Environmental Information (https://www.ncei.noaa.gov/data/sea-surface-temperature-optimum-interpolation/v2/access/avhrr-only/ (accessed on 19 May 2021)). Rainfall data is available at the official site of the India meteorological department (https://www.imdpune.gov.in/Clim_Pred_LRF_New/Grided_Data_Download.html (accessed on 6 August 2021)). Wind components are obtained from the C3S climate data store (https://cds.climate.copernicus.eu/cdsapp#!/dataset/reanalysis-era5-pressure-levels-monthly-means?tab=form (accessed on 23 May 2021)). Soil moisture, specific humidity and air temperature datasets are accessed via Giovanni (https://giovanni.gsfc.nasa.gov/giovanni/ (accessed on 10 May 2021)). Both Niño 3 SST index and dipole mode index were collected from climate time series developed by the GCOS surface pressure working group (https://psl.noaa.gov/gcos_wgsp/Timeseries/ (accessed on 28 June 2021)).

Acknowledgments: We thank Jingfeng Xiao and Xing Li for providing GOSIF data. We would like to thank NOAA, ECMWF, IMD, GMAO and LDAS for providing climate data used in this study. No external funding was received for the present work. We also thank anonymous reviewers and editors for their kind comments and suggestions.

Conflicts of Interest: The authors declare no conflict of interest.

References

1. Gonsamo, A.; Chen, J.M.; Lombardozzi, D. Global Vegetation Productivity Response to Climatic Oscillations during the Satellite Era. *Glob. Change Biol.* **2016**, *22*, 3414–3426. [CrossRef] [PubMed]
2. O'Carroll, A.G.; Armstrong, E.M.; Beggs, H.; Bouali, M.; Casey, K.S.; Corlett, G.K.; Dash, P.; Donlon, C.; Gentemann, C.L.; Høyer, J.L.; et al. Observational Needs of Sea Surface Temperature. *Front. Mar. Sci.* **2019**, *6*, 420. [CrossRef]
3. Phillips, H.E.; Tandon, A.; Furue, R.; Hood, R.; Ummenhofer, C.C.; Benthuysen, J.A.; Menezes, V.; Hu, S.; Webber, B.; Sanchez-Franks, A.; et al. Progress in Understanding of Indian Ocean Circulation, Variability, Air-Sea Exchange, and Impacts on Biogeochemistry. *Ocean Sci.* **2021**, *17*, 1677–1751. [CrossRef]
4. Ocean Health Index Sea Surface Temperature. Available online: https://oceanhealthindex.org/ (accessed on 23 January 2021).
5. Reimer, J.J.; Vargas, R.; Rivas, D.; Gaxiola-Castro, G.; Hernandez-Ayon, J.M.; Lara-Lara, R. Sea Surface Temperature Influence on Terrestrial Gross Primary Production along the Southern California Current. *PLoS ONE* **2015**, *10*, e0125177. [CrossRef] [PubMed]
6. Chen, M.; Parton, W.J.; DelGrosso, S.J.; Hartman, M.D.; Day, K.A.; Tucker, C.J.; Derner, J.D.; Knapp, A.K.; Smith, W.K.; Ojima, D.S.; et al. The Signature of Sea Surface Temperature Anomalies on the Dynamics of Semiarid Grassland Productivity. *Ecosphere* **2017**, *8*, e02069. [CrossRef]
7. Zhu, Z.; Piao, S.; Xu, Y.; Bastos, A.; Ciais, P.; Peng, S. The Effects of Teleconnections on Carbon Fluxes of Global Terrestrial Ecosystems. *Geophys. Res. Lett.* **2017**, *44*, 3209–3218. [CrossRef]
8. Nzabarinda, V.; Bao, A.; Xu, W.; Uwamahoro, S.; Jiang, L.; Duan, Y.; Nahayo, L.; Yu, T.; Wang, T.; Long, G. Assessment and Evaluation of the Response of Vegetation Dynamics to Climate Variability in Africa. *Sustainability* **2021**, *13*, 1234. [CrossRef]

9. Wang, J.; Wang, M.; Kim, J.S.; Joiner, J.; Zeng, N.; Jiang, F.; Wang, H.; He, W.; Wu, M.; Chen, T.; et al. Modulation of Land Photosynthesis by the Indian Ocean Dipole: Satellite-Based Observations and CMIP6 Future Projections. *Earth's Future* **2021**, *9*, 1–14. [CrossRef]
10. Kim, I.W.; Stuecker, M.F.; Timmermann, A.; Zeller, E.; Kug, J.S.; Park, S.W.; Kim, J.S. Tropical Indo-Pacific SST Influences on Vegetation Variability in Eastern Africa. *Sci. Rep.* **2021**, *11*, 10462. [CrossRef]
11. Frankenberg, C.; Berry, J. *Solar Induced Chlorophyll Fluorescence: Origins, Relation to Photosynthesis and Retrieval*; Elsevier: Amsterdam, The Netherlands, 2017; Volume 1–9, ISBN 9780128032206.
12. He, L.; Magney, T.; Dutta, D.; Yin, Y.; Köhler, P.; Grossmann, K.; Stutz, J.; Dold, C.; Hatfield, J.; Guan, K.; et al. From the Ground to Space: Using Solar-Induced Chlorophyll Fluorescence to Estimate Crop Productivity. *Geophys. Res. Lett.* **2020**, *47*, 1–12. [CrossRef]
13. Li, X.; Xiao, J.; He, B.; Altaf Arain, M.; Beringer, J.; Desai, A.R.; Emmel, C.; Hollinger, D.Y.; Krasnova, A.; Mammarella, I.; et al. Solar-Induced Chlorophyll Fluorescence is Strongly Correlated with Terrestrial Photosynthesis for a Wide Variety of Biomes: First Global Analysis Based on OCO-2 and Flux Tower Observations. *Glob. Change Biol.* **2018**, *24*, 3990–4008. [CrossRef]
14. Siegmann, B.; Cendrero-Mateo, M.P.; Cogliati, S.; Damm, A.; Gamon, J.; Herrera, D.; Jedmowski, C.; Junker-Frohn, L.V.; Kraska, T.; Muller, O.; et al. Downscaling of Far-Red Solar-Induced Chlorophyll Fluorescence of Different Crops from Canopy to Leaf Level Using a Diurnal Data Set Acquired by the Airborne Imaging Spectrometer HyPlant. *Remote Sens. Environ.* **2021**, *264*, 112609. [CrossRef]
15. Xu, S.; Atherton, J.; Riikonen, A.; Zhang, C.; Oivukkamäki, J.; MacArthur, A.; Honkavaara, E.; Hakala, T.; Koivumäki, N.; Liu, Z.; et al. Structural and Photosynthetic Dynamics Mediate the Response of SIF to Water Stress in a Potato Crop. *Remote Sens. Environ.* **2021**, *263*, 112555. [CrossRef]
16. Helm, L.T.; Shi, H.; Lerdau, M.T.; Yang, X. Solar-Induced Chlorophyll Fluorescence and Short-Term Photosynthetic Response to Drought. *Ecol. Appl.* **2020**, *30*, e02101. [CrossRef]
17. Hernández-Clemente, R.; Hornero, A.; Mottus, M.; Penuelas, J.; González-Dugo, V.; Jiménez, J.C.; Suárez, L.; Alonso, L.; Zarco-Tejada, P.J. Early Diagnosis of Vegetation Health from High-Resolution Hyperspectral and Thermal Imagery: Lessons Learned from Empirical Relationships and Radiative Transfer Modelling. *Curr. For. Rep.* **2019**, *5*, 169–183. [CrossRef]
18. Porcar-Castell, A.; Tyystjärvi, E.; Atherton, J.; Van Der Tol, C.; Flexas, J.; Pfündel, E.E.; Moreno, J.; Frankenberg, C.; Berry, J.A. Linking Chlorophyll a Fluorescence to Photosynthesis for Remote Sensing Applications: Mechanisms and Challenges. *J. Exp. Bot.* **2014**, *65*, 4065–4095. [CrossRef]
19. Liu, W.; Atherton, J.; Mõttus, M.; Gastellu-Etchegorry, J.P.; Malenovský, Z.; Raumonen, P.; Åkerblom, M.; Mäkipää, R.; Porcar-Castell, A. Simulating Solar-Induced Chlorophyll Fluorescence in a Boreal Forest Stand Reconstructed from Terrestrial Laser Scanning Measurements. *Remote Sens. Environ.* **2019**, *232*, 111274. [CrossRef]
20. Zhang, Y.; Xiao, X.; Jin, C.; Dong, J.; Zhou, S.; Wagle, P.; Joiner, J.; Guanter, L.; Zhang, Y.; Zhang, G.; et al. Consistency between Sun-Induced Chlorophyll Fluorescence and Gross Primary Production of Vegetation in North America. *Remote Sens. Environ.* **2016**, *183*, 154–169. [CrossRef]
21. Zhang, Y.; Joiner, J.; Hamed Alemohammad, S.; Zhou, S.; Gentine, P. A Global Spatially Contiguous Solar-Induced Fluorescence (CSIF) Dataset Using Neural Networks. *Biogeosciences* **2018**, *15*, 5779–5800. [CrossRef]
22. Geng, G.; Yang, R.; Liu, L. Downscaled Solar-Induced Chlorophyll Fluorescence Has Great Potential for Monitoring the Response of Vegetation to Drought in the Yellow River Basin, China: Insights from an Extreme Event. *Ecol. Indic.* **2022**, *138*, 108801. [CrossRef]
23. Peng, B.; Guan, K.; Zhou, W.; Jiang, C.; Frankenberg, C.; Sun, Y.; He, L.; Köhler, P. Assessing the Benefit of Satellite-Based Solar-Induced Chlorophyll Fluorescence in Crop Yield Prediction. *Int. J. Appl. Earth Obs. Geoinf.* **2020**, *90*, 102126. [CrossRef]
24. Hong, Z.; Hu, Y.; Cui, C.; Yang, X.; Tao, C.; Luo, W.; Zhang, W.; Li, L.; Meng, L. An Operational Downscaling Method of Solar-Induced Chlorophyll Fluorescence (SIF) for Regional Drought Monitoring. *Agriculture* **2022**, *12*, 547. [CrossRef]
25. Orth, R.; Seneviratne, S.I. Variability of Soil Moisture and Sea Surface Temperatures Similarly Important for Warm-Season Land Climate in the Community Earth System Model. *J. Clim.* **2017**, *30*, 2141–2162. [CrossRef]
26. Yan, B.; Mao, J.; Shi, X.; Hoffman, F.M.; Notaro, M.; Zhou, T.; McDowell, N.; Dickinson, R.E.; Xu, M.; Gu, L.; et al. Predictability of Tropical Vegetation Greenness Using Sea Surface Temperatures. *Environ. Res. Commun.* **2019**, *1*, 31003. [CrossRef]
27. Huang, M.; Wang, Z.; Wang, S.; Gu, F.; Gong, H.; Hao, M.; Shao, Y. Global Vegetation Productivity Responses to the West Pacific Warm Pool. *Sci. Total Environ.* **2019**, *655*, 641–651. [CrossRef]
28. Pereira, M.P.S.; Costa, M.H.; Justino, F.; Malhado, A.C.M. Response of South American Terrestrial Ecosystems to Future Patterns of Sea Surface Temperature. *Adv. Meteorol.* **2017**, *2017*, 2149479. [CrossRef]
29. Ying, K.; Peng, J.; Dan, L.; Zheng, X. Ocean—Atmosphere Teleconnections Play a Key Role in the Interannual Variability of Seasonal Gross Primary Production in China. *Adv. Atmos. Sci.* **2022**, *39*, 1329–1342. [CrossRef]
30. Huber, S.; Fensholt, R. Analysis of Teleconnections between AVHRR-Based Sea Surface Temperature and Vegetation Productivity in the Semi-Arid Sahel. *Remote Sens. Environ.* **2011**, *115*, 3276–3285. [CrossRef]
31. Sarkar, S.; Kafatos, M. Interannual Variability of Vegetation over the Indian Sub-Continent and Its Relation to the Different Meteorological Parameters. *Remote Sens. Environ.* **2004**, *90*, 268–280. [CrossRef]
32. Nayak, R.K.; Dadhwal, K.V.; Patel, N.R.; Dutt, C.B.S. Inter-Annual Variability of Net Ecosystem Productivity over India. *Int. Arch. Photogramm. Remote Sens. Spat. Inf. Sci.* **2012**, *XXXVIII-8/W20*, 125–128. [CrossRef]

33. Valsala, V.; Tiwari, Y.K.; Pillai, P.; Roxy, M.; Maksyutov, S.; Murtugudde, R. Intraseasonal Variability of Terrestrial Biospheric CO_2 Fluxes over India during Summer Monsoons. *J. Geophys. Res. Biogeosci.* **2013**, *118*, 752–769. [CrossRef]
34. Yadav, R.K.; Roxy, M.K. On the Relationship between North India Summer Monsoon Rainfall and East Equatorial Indian Ocean Warming. *Glob. Planet. Change* **2019**, *179*, 23–32. [CrossRef]
35. Asoka, A.; Mishra, V. Prediction of Vegetation Anomalies to Improve Food Security and Water Management in India. *Geophys. Res. Lett.* **2015**, *42*, 5290–5298. [CrossRef]
36. Sharma, A.; Goyal, M.K. Assessment of Ecosystem Resilience to Hydroclimatic Disturbances in India. *Glob. Chang. Biol.* **2018**, *24*, e432–e441. [CrossRef]
37. Nayak, R.K.; Patel, N.R.; Dadhwal, V.K. Inter-Annual Variability and Climate Control of Terrestrial Net Primary Productivity over India. *Int. J. Climatol.* **2013**, *33*, 132–142. [CrossRef]
38. Banger, K.; Tian, H.; Tao, B.; Ren, W.; Pan, S.; Dangal, S.; Yang, J. Terrestrial Net Primary Productivity in India during 1901–2010: Contributions from Multiple Environmental Changes. *Clim. Change* **2015**, *132*, 575–588. [CrossRef]
39. Nayak, R.K.; Patel, N.R.; Dadhwal, V.K. Spatio-Temporal Variability of Net Ecosystem Productivity over India and Its Relationship to Climatic Variables. *Environ. Earth Sci.* **2015**, *74*, 1743–1753. [CrossRef]
40. Bala, G.; Joshi, J.; Chaturvedi, R.K.; Gangamani, H.V.; Hashimoto, H.; Nemani, R. Remote Sensing Trends and Variability of AVHRR-Derived NPP in India. *Remote Sens.* **1982**, *5*, 810–829. [CrossRef]
41. Rao, A.S.; Bala, G.; Ravindranath, N.H.; Nemani, R. Multi-Model Assessment of Trends, Variability and Drivers of Terrestrial Carbon Uptake in India. *J. Earth Syst. Sci.* **2019**, *128*, 99. [CrossRef]
42. Kumar, A.; Pandey, V.; Shekh, A.M.; Lunagaria, M.M.; Patel, H.R. The Impact of El Nino and La Nina (ENSO) on Monsoon Rainfall in Gujarat Department of Agricultural Meteorology. *J. Agrometeorol.* **2012**, *14*, 151–156.
43. Deb Burman, P.K.; Sarma, D.; Chakraborty, S.; Karipot, A.; Jain, A.K. The Effect of Indian Summer Monsoon on the Seasonal Variation of Carbon Sequestration by a Forest Ecosystem over North-East India. *SN Appl. Sci.* **2020**, *2*, 154. [CrossRef]
44. Roxy, M. Sensitivity of Precipitation to Sea Surface Temperature over the Tropical Summer Monsoon Region and Its Quantification. *Clim. Dyn.* **2014**, *43*, 1159–1169. [CrossRef]
45. Ahmad, L.; Habib Kanth, R.; Parvaze, S.; Sheraz Mahdi, S. Agro-Climatic and Agro-Ecological Zones of India. In *Experimental Agrometeorology: A Practical Manual*; Ahmad, L., Habib Kanth, R., Parvaze, S., Sheraz Mahdi, S., Eds.; Springer International Publishing: Cham, Switzerland, 2017; pp. 99–118. ISBN 978-3-319-69185-5.
46. Qiu, R.; Han, G.; Ma, X.; Xu, H.; Shi, T.; Zhang, M. A Comparison of OCO-2 SIF, MODIS GPP, and GOSIF Data from Gross Primary Production (GPP) Estimation and Seasonal Cycles in North America. *Remote Sens.* **2020**, *12*, 258. [CrossRef]
47. Li, X.; Xiao, J. Mapping Photosynthesis Solely from Solar-Induced Chlorophyll Fluorescence: A Global, Fine-Resolution Dataset of Gross Primary Production Derived from OCO-2. *Remote Sens.* **2019**, *11*, 2563. [CrossRef]
48. Li, X.; Xiao, J. A global, 0.05-Degree Product of Solar-Induced Chlorophyll Fluorescence Derived from OCO-2, MODIS, and Reanalysis Data. *Remote Sens.* **2019**, *11*, 517. [CrossRef]
49. Xiao, J.; Li, X.; He, B.; Arain, M.A.; Beringer, J.; Desai, A.R.; Emmel, C.; Hollinger, D.Y.; Krasnova, A.; Mammarella, I.; et al. Solar-Induced Chlorophyll Fluorescence Exhibits a Universal Relationship with Gross Primary Productivity across a Wide Variety of Biomes. *Glob. Chang. Biol.* **2019**, *25*, e4–e6. [CrossRef]
50. Ranjan, A.K.; Dash, J.; Xiao, J.; Gorai, A.K. Vegetation Activity Enhanced in India during the COVID-19 Lockdowns: Evidence from Satellite Data. *Geocarto Int.* **2022**, *37*, 12618–12637. [CrossRef]
51. Chhabra, A.; Gohel, A. Elucidating Space Based Observations of Solar Induced Chlorophyll Fluorescence over Terrestrial Vegetation of India. *Trop. Ecol.* **2020**, *61*, 32–41. [CrossRef]
52. Huang, B.; Liu, C.; Banzon, V.; Freeman, E.; Graham, G.; Hankins, B.; Smith, T.; Zhang, H.M. Improvements of the Daily Optimum Interpolation Sea Surface Temperature (DOISST) Version 2.1. *J. Clim.* **2021**, *34*, 2923–2939. [CrossRef]
53. Reynolds, R.W.; Smith, T.M.; Liu, C.; Chelton, D.B.; Casey, K.S.; Schlax, M.G. Daily High-Resolution-Blended Analyses for Sea Surface Temperature. *J. Clim.* **2007**, *20*, 5473–5496. [CrossRef]
54. Banzon, V.; Smith, T.M.; Mike Chin, T.; Liu, C.; Hankins, W. A Long-Term Record of Blended Satellite and in Situ Sea-Surface Temperature for Climate Monitoring, Modeling and Environmental Studies. *Earth Syst. Sci. Data* **2016**, *8*, 165–176. [CrossRef]
55. Rayner, N.A.; Parker, D.E.; Horton, E.B.; Folland, C.K.; Alexander, L.V.; Rowell, D.P.; Kent, E.C.; Kaplan, A. Global Analyses of Sea Surface Temperature, Sea Ice, and Night Marine Air Temperature since the Late Nineteenth Century. *J. Geophys. Res. Atmos.* **2003**, *108*, 4407. [CrossRef]
56. Saji, N.H.; Yamagata, T. Possible Impacts of Indian Ocean Dipole Mode Events on Global Climate. *Clim. Res.* **2003**, *25*, 151–169. [CrossRef]
57. Gelaro, R.; McCarty, W.; Suárez, M.J.; Todling, R.; Molod, A.; Takacs, L.; Randles, C.A.; Darmenov, A.; Bosilovich, M.G.; Reichle, R.; et al. The Modern-Era Retrospective Analysis for Research and Applications, Version 2 (MERRA-2). *J. Clim.* **2017**, *30*, 5419–5454. [CrossRef]
58. GES-DISC. *Amy McNally NASA/GSFC/HSL (2018) FLDAS Noah Land Surface Model L4 Global Monthly 0.1 × 0.1 Degree (MERRA-2 and CHIRPS) (Version 001) [Dataset]*; Goddard Earth Sciences Data and Information Services Center (GES DISC): Greenbelt, MA, USA, 2018. [CrossRef]

59. Pai, D.S.; Sridhar, L.; Rajeevan, M.; Sreejith, O.P.; Satbhai, N.S.; Mukhopadhyay, B. Development of a New High Spatial Resolution (0.25° × 0.25°) Long Period (1901–2010) Daily Gridded Rainfall Data Set over India and Its Comparison with Existing Data Sets over the Region. *Mausam* **2014**, *65*, 1–18. [CrossRef]
60. Wilson, S.S.; Joseph, P.V.; Mohanakumar, K.; Johannessen, O.M. Interannual and Long Term Variability of Low Level Jetstream of the Asian Summer Monsoon. *Tellus A Dyn. Meteorol. Oceanogr.* **2018**, *70*, 1–9. [CrossRef]
61. Nandini, G.; Vinoj, V.; Pandey, S.K. Arabian Sea Aerosol-Indian Summer Monsoon Rainfall Relationship and Its Modulation by El-Nino Southern Oscillation. *NPJ Clim. Atmos. Sci.* **2022**, *5*, 25. [CrossRef]
62. Hersbach, H.; Bell, B.; Berrisford, P.; Hirahara, S.; Horányi, A.; Muñoz-Sabater, J.; Nicolas, J.; Peubey, C.; Radu, R.; Schepers, D.; et al. The ERA5 Global Reanalysis. *Q. J. R. Meteorol. Soc.* **2020**, *146*, 1999–2049. [CrossRef]
63. Minola, L.; Zhang, F.; Azorin-Molina, C.; Pirooz, A.A.S.; Flay, R.G.J.; Hersbach, H.; Chen, D. Near-Surface Mean and Gust Wind Speeds in ERA5 across Sweden: Towards an Improved Gust Parametrization. *Clim. Dyn.* **2020**, *55*, 887–907. [CrossRef]
64. Von Storch, H.; Zwiers, F. Testing Ensembles of Climate Change Scenarios for "Statistical Significance". *Clim. Change* **2013**, *117*, 1–9. [CrossRef]
65. Goswami, B.N.; Krishnamurthy, V.; Annmalai, H. A Broad-Scale Circulation Index for the Interannual Variability of the Indian Summer Monsoon. *Q. J. R. Meteorol. Soc.* **1999**, *125*, 611–633. [CrossRef]
66. Singh, M.; Bhatla, R. Intense Rainfall Conditions over Indo-Gangetic Plains under the Influence of Madden–Julian Oscillation. *Meteorol. Atmos. Phys.* **2020**, *132*, 441–449. [CrossRef]
67. Sahoo, M.; Kumar Yadav, R. The Interannual Variability of Rainfall over Homogeneous Regions of Indian Summer Monsoon. *Theor. Appl. Climatol.* **2022**, *148*, 1303–1316. [CrossRef]
68. Pathak, A.; Ghosh, S.; Alejandro Martinez, J.; Dominguez, F.; Kumar, P. Role of Oceanic and Land Moisture Sources and Transport in the Seasonal and Interannual Variability of Summer Monsoon in India. *J. Clim.* **2017**, *30*, 1839–1859. [CrossRef]
69. Roxy, M.K.; Ritika, K.; Terray, P.; Murtugudde, R.; Ashok, K.; Goswami, B.N. Drying of Indian Subcontinent by Rapid Indian Ocean Warming and a Weakening Land-Sea Thermal Gradient. *Nat. Commun.* **2015**, *6*, 7423. [CrossRef] [PubMed]
70. Osakabe, Y.; Osakabe, K.; Shinozaki, K.; Tran, L.-S.P. Response of Plants to Water Stress. *Front. Plant Sci.* **2014**, *5*, 86. [CrossRef]
71. Costa de Oliveira, A.; Marini, N.; Farias, D.R. *Climate Change: New Breeding Pressures and Goals*; Elsevier Ltd.: Amsterdam, The Netherlands, 2014; Volume 2, ISBN 9780080931395.
72. Singh, S.K.; Reddy, V.R.; Devi, M.J.; Timlin, D.J. Impact of Water Stress under Ambient and Elevated Carbon Dioxide across Three Temperature Regimes on Soybean Canopy Gas Exchange and Productivity. *Sci. Rep.* **2021**, *11*, 16511. [CrossRef]
73. Zhou, Z.Q.; Xie, S.P.; Zhang, R. Variability and Predictability of Indian Rainfall during the Monsoon Onset Month of June. *Geophys. Res. Lett.* **2019**, *46*, 14782–14788. [CrossRef]
74. Sharma, A.; Goyal, M.K. District-Level Assessment of the Ecohydrological Resilience to Hydroclimatic Disturbances and Its Controlling Factors in India. *J. Hydrol.* **2018**, *564*, 1048–1057. [CrossRef]
75. Xu, H.J.; Wang, X.P. Effects of Altered Precipitation Regimes on Plant Productivity in the Arid Region of Northern China. *Ecol. Inform.* **2016**, *31*, 137–146. [CrossRef]
76. Zhu, Y.; Luo, P.; Zhang, S.; Sun, B. Spatiotemporal Analysis of Hydrological Variations and Their Impacts on Vegetation in Semiarid Areas from Multiple Satellite Data. *Remote Sens.* **2020**, *12*, 4177. [CrossRef]
77. Ji, Y.; Zhou, G.; Luo, T.; Dan, Y.; Zhou, L.; Lv, X. Variation of Net Primary Productivity and Its Drivers in China's Forests during 2000–2018. *For. Ecosyst.* **2020**, *7*, 15. [CrossRef]
78. Pathak, A.; Ghosh, S.; Kumar, P.; Murtugudde, R. Role of Oceanic and Terrestrial Atmospheric Moisture Sources in Intraseasonal Variability of Indian Summer Monsoon Rainfall. *Sci. Rep.* **2017**, *7*, 12729. [CrossRef] [PubMed]